

Mesoscale Convective Systems and Critical Clusters

OLE PETERS AND J. DAVID NEELIN

*Department of Atmospheric and Oceanic Sciences, and Institute of Geophysics and Planetary Physics,
University of California, Los Angeles, Los Angeles, California*

STEPHEN W. NESBITT

Department of Atmospheric Sciences, University of Illinois at Urbana–Champaign, Urbana, Illinois

(Manuscript received 14 February 2008, in final form 27 August 2008)

ABSTRACT

Size distributions and other geometric properties of mesoscale convective systems (MCSs), identified as clusters of adjacent pixels exceeding a precipitation threshold in satellite radar images, are examined with respect to a recently identified critical range of water vapor. Satellite microwave estimates of column water vapor and precipitation show that the onset of convection and precipitation in the tropics can be described as a phase transition, where the rain rate and likelihood of rainfall suddenly increase as a function of water vapor. This is confirmed in Tropical Rainfall Measuring Mission radar data used here. Percolation theory suggests that cluster properties should be highly sensitive to changes in the density of occupied pixels, which here translates into a rainfall probability, which in turn sensitively depends on the water vapor. To confirm this, clusters are categorized by their prevalent water vapor. As expected, mean cluster size and radius of gyration strongly increase as the critical water vapor is approached from below. In the critical region one finds scale-free size distributions spanning several orders of magnitude. Large clusters are typically from the critical region: at low water vapor most clusters are small, and supercritical water vapor values are too rare to contribute much. The perimeter of the clusters confirms previous observations in satellite, field, and model data of robust nontrivial scaling. The well-known area–perimeter scaling is fully compatible with the quantitative prediction from the plausible null model of gradient percolation, where the accessible hull is a fractal object with dimension $4/3$.

1. Introduction

Mesoscale convective systems (MCSs) have been the object of much study because of their importance for severe weather and rainfall production (Cotton and Anthes 1989; Houze 2004). One common tool in studying these systems has been to examine clusters of connected pixels for radar, microwave, or infrared indicators of cloud. Working definitions of MCSs are phrased in terms of such clusters—for example, an area of brightness temperature below 250 K of at least 2000 km² (Mohr and Zipser 1996) or a linear dimension of at least 100 km in one direction (Houze 1993; Geerts 1998; Nesbitt et al. 2006), plus the widely met criterion of strong convection within the cluster. The size distribu-

tion of these clusters (where “size” refers to the horizontal area) has often been described as lognormal (López 1977; Houze and Cheng 1977; Cheng and Houze 1979; Williams and Houze 1987; Houze 1993), although recent data (Mapes and Houze 1993; Nesbitt et al. 2006) indicate that the correspondence to lognormal is rather loose. Cahalan and Joseph (1989), Benner and Curry (1998), and Neggers et al. (2003) have all postulated power-law size distributions for clouds. We will use the term “precipitation cluster” for any collection of adjacent radar pixels indicating precipitation (radar reflectivity ≥ 20 dBZ) because the clusters discussed do not all meet the traditional size criterion for MCS.

Recently Peters and Neelin (2006, hereafter PN06) noted that the transition to strong precipitation in the tropics exhibits properties of nonequilibrium continuous phase transitions, for which there exists an extensive literature (see review by Hinrichsen 2000). Using Tropical Rainfall Measuring Mission (TRMM) Microwave

Corresponding author address: Ole Peters, 405 Hilgard Ave.,
Los Angeles, CA 90095–1565.
E-mail: ole@santafe.edu

Imager (TMI) data for column integrated water vapor and microwave-estimated precipitation (Wentz and Spencer 1998), they showed a sharp increase in precipitation above a critical value of the water vapor. The functional form of the increase above criticality was consistent with a power law. In the parlance of continuous phase transitions, the water vapor was interpreted as a tuning parameter and the precipitation rate as an order parameter. Near criticality, the variance of the order parameter (a measure of thermodynamic susceptibility) was found to peak strongly, and a finite-size scaling analysis revealed long-range (power law) correlations in the precipitation field, all in agreement with the theory of continuous phase transitions. We will refer to this transition as the precipitation transition for brevity, with the understanding that in cases studied here the transition is associated with the transition to strong deep convection.

The fact that long-range spatial correlation persisted over the observed spectrum of scales (up to several hundred kilometers) suggests that spatially structured objects exist at least up to this scale. Meteorologically, PN06 suggested that these objects are likely to correspond to MCSs, relating them to critical clusters in other systems (Stauffer and Aharony 1994). Here we seek to confirm and quantify a change in properties of tropical mesoscale convective clusters associated with the precipitation transition identified in PN06, using the cluster algorithm of Nesbitt et al. (2006) for TRMM 2A25 radar data, for which the mesoscale cluster properties have already been established with respect to traditional mesoscale meteorological approaches. From the mesoscale modeling literature, there are indications that tropospheric water vapor can affect tropical rainfall characteristics in general (Bretherton et al. 2004), and MCSs in particular (Lucas et al. 2000; Tompkins 2001; Houze et al. 2007), with some support in conventional observational diagnostics (LeMone et al. 1998).

Given the strong dependence of rainfall probability on water vapor, and the expected sensitive dependence of cluster properties on rainfall probability, we anticipate a change in cluster properties as the water vapor crosses the critical point.

Thermodynamic issues are commonly discussed in terms of geometric properties of spatial domains. For example, the critical behavior of the Ising model, a mathematical caricature of a ferromagnet, can be formulated in terms of geometric properties of clusters of aligned spins. Its free energy functional can be written as a summation over different configurations of domain walls (Cardy 2005). For an introductory review, see chapter 7 of Stauffer and Aharony (1994). From this literature we extract the caveat that certain geometric

properties (for instance, area–perimeter scaling, the statistical dependence of the perimeter of a cluster on its area; see below) are so robust that they are insensitive to the physical processes that generate them. These properties can easily be predicted, but they tell us little about the physics behind them. Whenever spatial clusters are important in the statistical description of a system, a comparison to the null model of spatial clustering—percolation—is worthwhile. In the present context, we have to deal with the added difficulty of inhomogeneity, both in water vapor [here measured by the column integrated water vapor $w(\mathbf{x}, t)$, where \mathbf{x} denotes the location and t is time] and in the resulting rain field. The lessons from percolation theory will therefore be largely reduced to qualitative statements. These do, however, set hypotheses for the behavior of precipitation cluster statistics as a function of water vapor, which we can then test. We emphasize that predictions from the null model of percolation are complementary to a perspective rooted in the physics of mesoscale systems in that they only make use of geometry. Departures from percolation can be a starting point from which to investigate the physics.

Before we describe the setup of percolation, we note its importance here not only as an extremely simple model of spatial clustering but also as an extremely simple model with a continuous phase transition. We first recap geometric properties that are of interest for our study and then discuss the limitations of the comparison between MCSs and percolation clusters.

In its simplest form, percolation theory is concerned with regular lattices whose sites are occupied with a uniform probability p (Stauffer and Aharony 1994). The resulting discrete fields of occupied and empty sites are spatially uncorrelated. Nonetheless, the clusters of adjacent occupied sites that arise have a highly complex fractal spatial structure. At low concentration of occupied sites, clusters are typically small, and large agglomerations are exponentially unlikely. As p is increased, however, typical cluster sizes grow until the critical point is reached, $p = p_c$, where percolation occurs: In a system whose linear size L approaches infinity, a cluster spans the system, providing paths of occupied nearest-neighbor sites between opposing system boundaries. In the thermodynamic limit $L \rightarrow \infty$, the average cluster size $\langle s \rangle (p)$ diverges as a power law as p_c is approached:

$$\lim_{p \rightarrow p_c} \langle s \rangle (p) = a_s^\pm |p - p_c|^{-\gamma}, \quad \text{for } p \text{ close to } p_c, \quad (1)$$

where a_s^\pm denotes the proportionality factors for $p < p_c$ and $p > p_c$. The average radius of gyration $\langle r \rangle (p)$, a useful measure of the effective radius for geometrically complex objects [see Eq. (6)], diverges similarly:

$$\lim_{p \rightarrow p_c} \langle r \rangle(p) = a_r^\pm |p - p_c|^{-\nu}, \quad \text{for } p \text{ close to } p_c. \quad (2)$$

The ensemble considered for the averages does not include any spanning clusters (clusters that connect opposing system boundaries). Including such clusters, the average cluster size would tend to infinity for any $p \geq p_c$ in the thermodynamic limit. The factors a_s^\pm and a_r^\pm are nonuniversal; that is, they depend on microscopic details like the lattice structure (triangular, hexagonal, square, etc.). The exponent γ (as well as amplitude ratios, such as a_s^+/a_s^-), on the other hand, are universal to all percolation systems, depending only on the dimensionality of the lattice. For finite systems at criticality, the distribution of cluster sizes is cut off at an L -dependent characteristic size $s_\xi \propto L^D$, which dominates the average cluster size. The divergences (1) and (2) are then capped because there cannot be an infinite cluster in a finite system.

The size distribution of clusters at the critical point, $p = p_c$, is scale-free:

$$n_s(s; L) = s^{-\tau} \mathcal{G}(s/s_\xi), \quad (3)$$

where $n_s(s)$ denotes the ‘‘cluster number’’ or probability density of a given cluster having size s . In finite systems, the cluster size distribution is cut off by a scaling function $\mathcal{G}(s/s_\xi)$ with the single argument s/s_ξ . Clusters larger than the characteristic size s_ξ are extremely unlikely: $\forall n, \lim_{s \rightarrow \infty} s^n \mathcal{G}(s/s_\xi) = 0$. This expression simply means that none of the moments of the size distribution diverge, which is necessarily true for any finite system. The function $\mathcal{G}(x)$ is further required to be infinitely differentiable and to be constant for small arguments: $\lim_{x \rightarrow 0} \mathcal{G}(x) = \text{const}$. In the thermodynamic limit one thus recovers the pure power-law behavior. As s_ξ diverges, the argument $x = s/s_\xi$ approaches zero, and $n_s(s) = \text{const} \times s^{-\tau}$. Otherwise, $\mathcal{G}(x)$ is a priori quite arbitrary and can take various shapes, depending, for example, on the aspect ratio of the system (Moloney and Pruessner 2003).

The critical exponents γ , ν , and τ are universal to all two-dimensional percolation problems. In practice we observe (from small to large clusters) a distribution that starts out fairly arbitrary, then follows a power law over a range that depends on the system size, and finally decays very fast (e.g., like an exponential). For this reason, the ‘‘true’’ (infinite system) behavior of $n_s(s)$ is sometimes difficult to infer from observations. For example, the universal exponent τ can in principle be read off a double-logarithmic plot as the negative slope in the power-law regime. However, the change from the power-law regime to the cutoff regime is often gradual, which can produce a continuously changing slope, making it

impossible to ascribe a single value to the exponent. To address these problems systematically, a finite-size scaling analysis would be required, where the system size is changed in a controlled way and the spatial structure of $p(\mathbf{x})$ is known precisely. This, however, is beyond the scope of the present paper.

In studies of clusters in continuous phase transitions (like the percolation transition), the tuning field that controls the phase transition [in percolation $p(\mathbf{x})$ is usually homogeneous in space. In a field with strong inhomogeneities, such as the environment that controls the emergence of precipitation clusters (or MCSs), we can only expect the most robust homogeneous properties to survive. For example, we mentioned that system-spanning clusters are removed from any averages. Above percolation criticality only small clusters occur in the holes of the infinite (or spanning) cluster. The infinite cluster has a very small density near the phase transition, and many holes exist. In the case of precipitation clusters, however, we expect meteorologically that the interior of a cluster is quite dense. Clusters from the holes of other clusters therefore contribute negligibly to the statistics. Furthermore, although we remove clusters that span the radar swath, spanning criteria that take into account the inhomogeneities have not been developed—for instance, one could remove clusters that span a region of elevated water vapor. The supercritical behavior of Eq. (1) is thus not expected to be reproduced. Approaching the transition from below, the average cluster size will sharply increase, but it is unlikely to decrease above criticality.

We can make a very robust prediction about MCS perimeters based on a setup called gradient percolation (Gouyet and Rosso 2005). Consider a two-dimensional square lattice (with spatial coordinates x and y) of length L whose occupation probability is a function of one spatial coordinate. It is fully occupied at one end, $p(0, y) = 1$, from where the occupation probability decreases linearly in x to $p(L, y) = 0$. Clearly, there will be a cluster connecting the bottom ($y = 0$) to the top ($y = L$) at $x = 0$. There will certainly be no such cluster at $x = L$, where the occupation probability is zero. Somewhere in between there must therefore be a boundary, called the hull, of the cluster that spans from top to bottom. The fractal dimension of this boundary depends on the precise definition of the hull. For the most robust object (Kolb 1990), which is known as the ‘‘accessible hull,’’ it is $d_f = 4/3$. This object is a particular kind of perimeter, the details of which can be important, as we discuss in section 6.

The robustness of the prediction for the accessible hull dimension can be understood as follows: Although other quantitative results crucially depend on a good

estimate of the relevant occupation probability $p(\mathbf{x})$ in the environment that a given cluster inhabits, this is not the case for the hull dimension. As long as the spatial dependence of $p(\mathbf{x})$ can be linearized in the vicinity of the perimeter, the result holds. The precise morphology of the clusters is thus not important—instead of a gradient along one dimension, this would apply for an MCS that is healthy [high $p(\mathbf{x})$] in the center, with conditions becoming progressively less favorable [decreasing $p(\mathbf{x})$] as one moves out to the surrounding environment. An explicit measurement of $p(\mathbf{x})$ is not required. On average, the water vapor at the center of a cluster, and therefore the likelihood for convection and precipitation, is higher than in the area surrounding the cluster.

Apart from the very robust exponent just described, we do not attempt to relate apparent exponents to specific models or processes. This would require knowledge of the spatial structure of any inferred precipitation probability $p(\mathbf{x})$.

Above the critical water vapor w_c , both the average rain intensity and the probability of observing 20-dBZ radar reflectivity increase sharply. With respect to clusters of precipitating pixels, this is akin to the occupation probability p in percolation problems. Geometric critical phenomena of the type described above will occur near w_c (because p changes quickly here), with the precise point in w determined by the particular cutoff value for considering a pixel as precipitating (here 20 dBZ). If the convective and geometric critical points do not occur at precisely the same value of water vapor, then much of the observed geometric behavior will be unaffected by the physical processes. This has the advantage that geometric properties of rain fields can be understood without knowledge of precipitation physics, but it has the disadvantage that geometric properties have little discriminative power with respect to physical processes.

2. Data and methods

Version 6 TRMM precipitation radar (PR) data from algorithm 2A25 (Iguchi et al. 2000) from 1 January 1998 through 31 December 2006 were used in the present analysis. About 16 million clusters were analyzed. A modified version of the algorithm described by Nesbitt et al. (2006) was used to identify precipitation features—clusters of contiguous pixels exceeding a given reflectivity. The modifications are as follows: (i) Only the PR near-surface reflectivity field was used to identify contiguous pixels >20 dBZ (no microwave imager data were used in the grouping) and (ii) next-nearest-neighbor pixels were not included in the feature grouping (i.e., only adjacent pixels were included). The latter modification was done to match common practice in the percolation literature

(Stauffer and Aharony 1994). For each identified feature, the area, full and accessible hull lengths, and the radius of gyration were computed. The area of each feature was calculated by summing the number of pixels and multiplying by the nominal PR instrument field of view [$(4.23 \text{ km})^2$ before 8 August 2001 and $(5.0 \text{ km})^2$ afterward]. These values were computed as the mean area projected by the PR pixel centroids as if it were a square lattice. The full hull length was calculated by walking along the edges of all boundary pixels of a given feature in counterclockwise direction, summing the distance traveled until the starting point is reached. Accessible hull length is calculated in a similar way, except that gaps less than one pixel in width are treated as cells on the feature boundary; long fjords into the features are thereby cut off. The radius was computed as described below [see Eq. (6)]. Each cluster was associated with the precipitable water value from the TMI pixel that contains the cluster centroid. The TMI resolution is about 25 km, compared to the radar's approximately 5 km, so this samples a square of about 25 radar pixels characterizing the interior environment for large clusters, with the caveat for small clusters that some exterior environment is inevitably sampled as well. This "centroid-surrounding value" seems the most appropriate choice, within the resolution limitations. The cluster statistics are then binned for each 1-mm interval in water vapor. For removal of spanning clusters, we have implemented the criterion of spanning the radar swath [215 (247) km wide before (after) 1 August 2001], which would be appropriate in a homogeneous water vapor environment, with caveats discussed below. In some cases (Figs. 4, 5, 7, and 8) swath-spanning clusters were removed, but clusters touching one side of the swath were left in the ensemble. Elsewhere (Figs. 6 and 9) the restrictions on data are even stricter: boundary-touching clusters are also removed because the swath would introduce artificially straight sections of accessible hull.

To compute nongeometric properties, in particular the ensemble-average radar precipitation rate as a function of precipitable water, the 2A25 radar rain rates were averaged onto the TMI water vapor grid (0.25° latitude \times 0.25° longitude).

Following PN06, all analyses were carried out for four major tropical (20°S to 20°N) ocean basins, the western Pacific (120°E – 170°W), eastern Pacific (170° – 70°W), Atlantic (70°W – 20°E), and Indian (30° – 120°E) Oceans.

3. The precipitation transition in radar precipitation data

A first major step is to establish that the transition seen in PN06 in microwave precipitation retrievals is

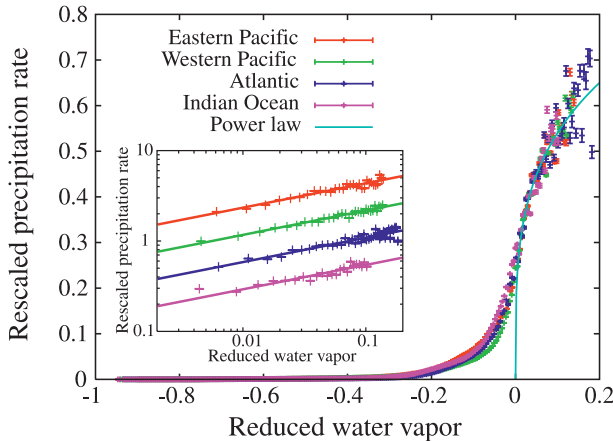


FIG. 1. Radar-derived rescaled precipitation rates conditionally averaged as a function of the dimensionless reduced water vapor $(w_c^i - w)/w_c^i$, where w_c^i denotes the critical water vapor in the four tropical regions i defined in section 2. (inset) The pickup is well described by a power law, as expected for a continuous phase transition. The vertical axis is the precipitation rate in arbitrary units, chosen to offset individual curves. Error bars are standard errors in each w bin.

found in the radar retrievals. Specifically, we expect that above a critical value of the column water vapor w_c , the ensemble average precipitation as a function of w will approach

$$\langle P \rangle(w) = a(w - w_c)^\beta \quad (4)$$

from a region of opposite curvature starting below w_c that is due to spatiotemporal inhomogeneity effects, finite-size effects, or effects of variables other than w . We also expect a steep drop in the frequency of occurrence of a given value of w for $w > w_c$. The power-law pickup of the precipitation above w_c in Fig. 1 (where w_c is determined as discussed below) shows remarkable agreement with that established from the microwave data in PN06. The amplitudes of the TMI Wentz algorithm rainfall are significantly higher, which may be of interest for the comparison of rainfall algorithms; however, in the language of continuous phase transitions, such amplitudes are nonuniversal and not of primary interest from this point of view. The exponent 0.265 of the power law shown in the inset of Fig. 1 is the average of the best-fit values for β for the different regions. We used the following fitting procedure: Choose a fitting range $[w^*: 75 \text{ mm}]$, 75 mm being the highest recorded value of w and w^* being an index for the iteration in the fitting procedure. Find the values for $w_c < w^*$, β , and a that minimize the χ^2 in log–log space between the data and Eq. (4). Repeating this for all possible w^* [0 mm: 75 mm] yields the minima χ_{\min}^2 as a function of w^* . Now divide each minimum by the number of terms contrib-

uting to the χ^2 sum. This “error per data point” is a nonmonotonic function for the data, and the minima indicate the best-fit values of w_c , β , and a . From the differences in χ_{\min}^2 we estimate an error bar of about ± 0.04 for β . This result is compatible within error bars with the exponent estimated in PN06, where $\beta = 0.215 \pm 0.02$ was found (with a slightly different algorithm). It indicates that there is no significant net effect from the processes that distinguish radar from microwave-inferred estimates of rainfall intensity on the universal value of the power-law exponent. The radar and microwave measurements do not agree in terms of amplitudes [a in Eq. (4)]. The average estimated rain rate at a given water vapor above criticality is typically about 4 times larger in the TMI (Wentz and Spencer 1998) dataset used in PN06. However, the latest release by Remote Sensing Systems of the TMI data, using an improved algorithm by Hilburn and Wentz (2008), scales the rain rates down considerably. The best-fit critical values w_c are 65.6, 65.7, 63.2, and 67.8 mm, respectively, for the eastern Pacific, western Pacific, Atlantic, and Indian Oceans. They agree to ± 1.9 mm with the values found in PN06.

The agreement of the radar with the microwave retrievals in β and w_c has substantial implications for the physics of the precipitation transition. It implies that large hydrometeors with nonnegligible fall speeds are involved, whereas from the TMI retrievals the partition into rain and cloud water depended on algorithm assumptions. The radar data further help reject the possibility that the change in curvature above w_c in Fig. 1 is due to an upper cutoff in recorded rain rates. The estimation of rain rates based on TRMM PR reflectivity profiles includes several crucial steps—such as correcting for attenuation and modeling drop size distributions, with their respective uncertainties (Iguchi et al. 2000)—but neither the retrieval algorithm nor the data recording imposes a hard-wired upper cutoff on the radar rain rates.

For cluster properties it is most important that the probability for counting a pixel in a radar image as occupied increases rapidly with the water vapor in the area of the pixel. In Fig. 2 we thus quantify the dependence of this occupation probability (for a radar pixel to exceed the reflectivity threshold) on the water vapor at the TMI pixel in which it occurs. A very steep increase occurs near the critical point w_c of the precipitation transition. For reference, the critical occupation probability for two-dimensional site percolation in a homogeneous square lattice is $p_c^{\text{square}} \approx 0.5927$. We caution that an effective p_c in our case will be different because of physical effects. The arbitrariness of the 20-dBZ threshold value makes it unlikely that p_c will correspond exactly to

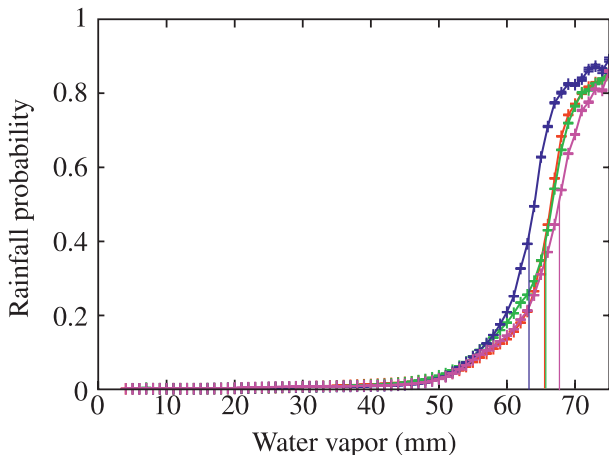


FIG. 2. Relative frequency of pixels surpassing the 20-dBZ reflectivity threshold as a function of water vapor w for the four tropical regions defined in section 2. We refer to this as the rainfall or occupation probability, $p(w)$. Standard errors are shown where they are wider than the line width. At w values near the precipitation transition (Fig. 1; critical water vapor values w'_c are indicated as vertical straight lines), the occupation probability increases rapidly.

the precipitation-critical point w_c . However, the steepness of the occupation probability increase ensures that any reasonable critical value of occupation probabilities is reached near the precipitation transition.

Figure 3 shows the frequencies of occurrence of different levels of water vapor in the investigated tropical regions. The distributions are very clearly different, reflecting climatic differences. We will argue below that cluster size distributions (just as precipitation rates) conditioned on specific levels of water vapor have universal features. Because in many studies the cluster size distributions are effectively weighted by the nonuniversal distributions of water vapor, the universal properties are not observed.

4. Mean cluster size and radius of gyration

We define the mean cluster size $\langle s \rangle(w)$ as the first moment of the observed cluster sizes s_i with corresponding binned water vapor w_i , conditioned on some value of the water vapor $w \in \{w_i\}$:

$$\langle s \rangle(w) = \frac{\sum_i s_i \delta(w_i, w)}{\sum_i \delta(w_i, w)}, \quad (5)$$

with the Kronecker delta $\delta(x, y) = 0, 1$ if $x \neq y$ and $x = y$, respectively. We express the size in km^2 . The radius of gyration r is the root-mean-square distance of (the midpoints of) all cluster sites j from the centroid \mathbf{x}_{CM} :

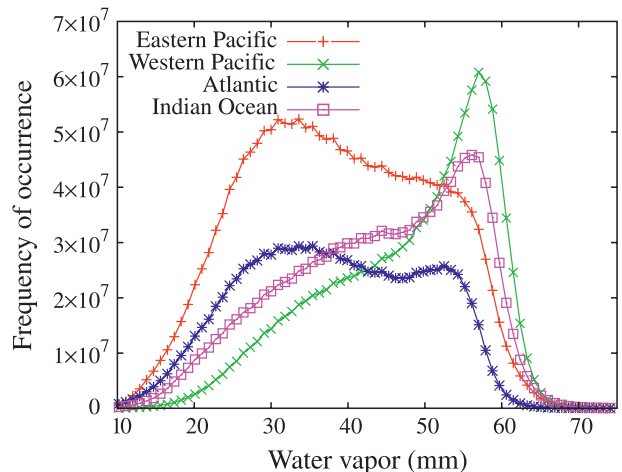


FIG. 3. Frequencies of occurrence of water vapor values (in bins of 0.3 mm) during the entire measurement period for the same tropical regions as in Fig. 1. Standard errors are smaller than the line width.

$$\mathbf{x}_{\text{CM}} = \frac{\sum_j \mathbf{x}_j}{\sum_j 1} \quad (6)$$

$$r^2 = \frac{\sum_j |\mathbf{x}_j - \mathbf{x}_{\text{CM}}|^2}{\sum_j 1}.$$

The conditional average radius of gyration $\langle r \rangle(w)$ is defined equivalently to the mean cluster size, replacing s_i by r_i in Eq. (5).

As mentioned above, these quantities are expected to increase sharply near the critical point, and indeed they do, as seen in Figs. 4 and 5. The increase in both quantities occurs at a lower water vapor level in the Atlantic, roughly corresponding to the lower value of w_c in that basin. This also implies that the Atlantic statistics have larger estimation error at higher water vapor levels because the frequency of occurrence decreases rapidly near and above criticality (Fig. 3). In homogeneous systems there would be a maximum at criticality because we removed from the sample any clusters spanning the radar swath. In the present (considerably inhomogeneous) system we observe large fluctuations and a slight further increase as the tuning parameter surpasses its likely critical value. The strong inhomogeneities in the w field make the clusters more compact in the interior. Holes in which smaller clusters could live are rare and only large clusters contribute to the average. Thus, the compactness of clusters can lead to a continued increase in the average cluster size above criticality. We removed spanning clusters to facilitate comparison with studies in

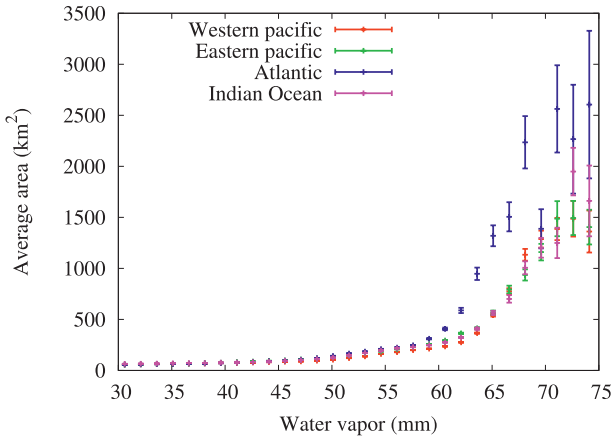


FIG. 4. The mean cluster size as a function of column water vapor w for the four tropical regions defined in section 2. Average sizes are dominated by single-pixel clusters for low water vapor values and pick up dramatically, with large fluctuations, as the critical water vapor level is surpassed. Standard errors are shown.

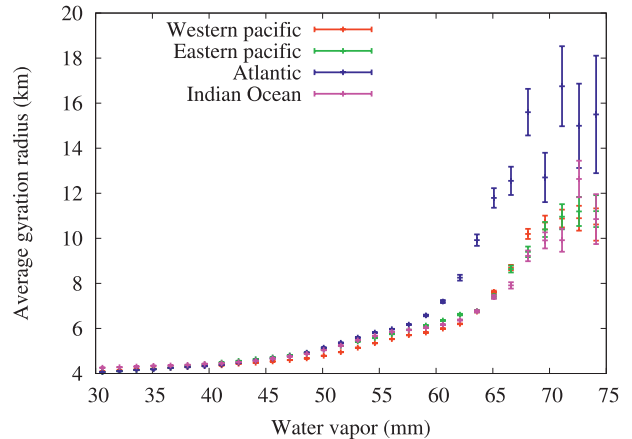


FIG. 5. The radius of gyration of as a function of column water vapor w for the four tropical regions defined in section 2. For low water vapor values, the average radius is dominated by clusters consisting of one pixel ($r \approx 3$ km). Near the precipitation transition, clusters with larger radii emerge. Standard errors are shown.

statistical mechanics. The small effect of this procedure indicates that the inhomogeneities in the system are a stronger constraint than the swath width.

Figure 6 supports the view that the clusters are compact objects because their gyration radius scales trivially as the square root of the area. For a fractal object this would not be the case. It is important to point out, however, that percolation clusters are quite compact (their fractal dimension is $91/48 \approx 1.9$) and it is not possible to distinguish these two behaviors from this figure alone. The blue straight line in Fig. 6 indicates the minimum possible radius of gyration for a given cluster size—that of a perfect disk with equal area. The red line is the maximum possible radius—that of a straight line whose width is given by the pixel size. Not surprisingly (for the 20-dBZ threshold used here, which tends to include cloud shields for squall line structures), clusters are closer to being disks than lines. Very large clusters tend to be slightly elongated, which could result from limits imposed by the swath width.

5. Water vapor dependence of cluster size distributions

Purely based on a diverging correlation length, in a system approximating a continuous phase transition we expect a range of scales that exhibit scale-free behavior near criticality—in our case, a range of convective cluster sizes distributed according to a power law. Because there is evidence for a diverging correlation length, for example in the finite-size scaling analysis in PN06, we might expect scale freedom based on the dynamics of the system. However, we also expect a

geometric contribution to the clusters. Such a combination of geometric and physical criticality also arises in the Ising model, where “there are two contributions to the [...] clusters: one is due to the correlations [in our case, convective physics], and the other is due to purely geometric effects” (Coniglio and Klein 1980). In our case both contributions are expected to depend strongly on water vapor. We thus investigate clusters at different water vapors, asking which properties merely reflect those of percolation. Observed properties that differ from those of percolation indicate a significant effect of the physical contribution.

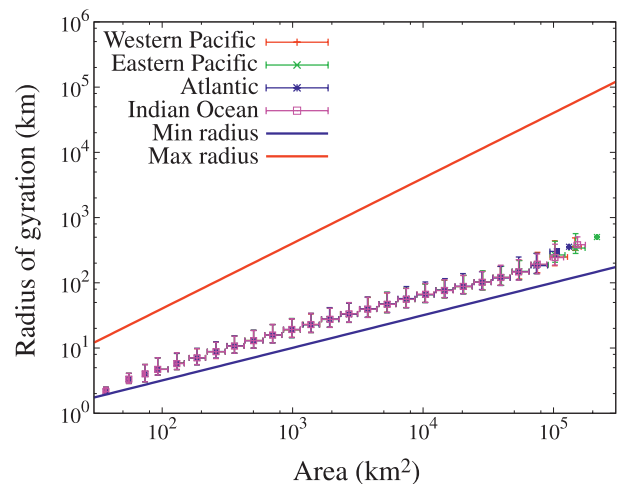


FIG. 6. The median radius of gyration vs the median cluster size for the four tropical regions defined in section 2. Vertical and horizontal bars range from the 5th to 95th percentile in bins defined by the cluster size.

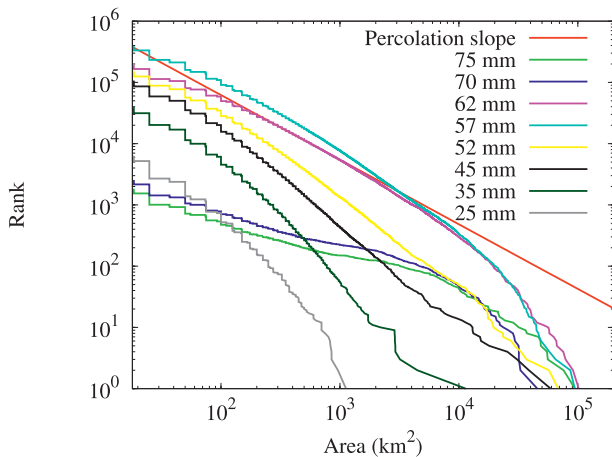


FIG. 7. Rank of clusters as a function of cluster size (number of clusters larger than a given size in km^2) for various values of the centroid water vapor, shown for the western Pacific. For the most frequent water vapor values, the distribution has a scale-free range. Apparent exponents (log-log slopes) are close to the 2D percolation slope of $-\tau + 1 = -187/91 + 1$ for the rank distribution.

As discussed in section 1, even for systems much simpler than the atmosphere it is a difficult task to measure the scaling behavior. To the usual complications are added potential impacts of inhomogeneity in water vapor and the competition between properties of the purely geometric phase transition and the nearby physical precipitation transition. The physical MCSs are generated by the transition to strong convection, and one would expect the precipitation-critical point to coincide with that of percolation. However, the geometric properties examined here depend on the 20-dBZ threshold, so the geometric phase transition need not occur at exactly the same point as the precipitation transition (although the rapidity of the radar pickup as a function of water vapor will tend to keep them close for reasonable choices of threshold). In PN06, long-range correlation associated with the precipitation transition was found as far as 20 mm in water vapor away from criticality. Another problem is the influence of other unobserved atmospheric variables, such as tropospheric temperature, that also have an effect on the likelihood of precipitation.

Bearing this in mind, we expect to find a regime near w_c with scale-free cluster-size distributions (up to a cutoff set by swath width and water vapor inhomogeneity) and a regime well below w_c where cluster sizes decay fast beyond a characteristic size smaller than the hard limit set by the system size. The observed cluster size distributions in Figs. 7 and 8 follow these expectations. Size distributions of small clouds are often fitted to double power laws, using one exponent up to some

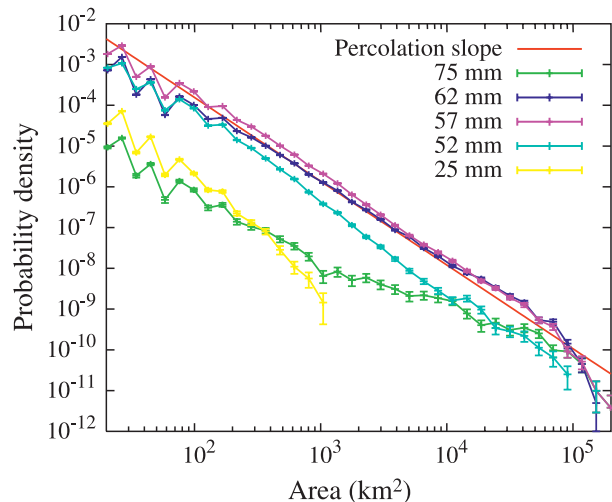


FIG. 8. The probability density function for a randomly selected cluster to be of a given size. Normalization is over all water vapor values. We show data for the western Pacific for various water vapor values at the centroid of the cluster. Two extreme cases, $w^{\max} = 75$ and $w^{\min} = 25$, are shown. These cases differ considerably from percolation-type scaling. For water vapor values in the critical region, however, a power law with percolation exponent ($-187/91$) is an acceptable approximation to the data (red line). We therefore cannot exclude the possibility that the nontrivial character of mesoscale convective cluster size distributions is a result of a percolation transition. Error bars show standard errors in each bin. For small clusters, we see systematic effects due to the lattice resolution and structure.

scale and another, steeper exponent from there on (Cahalan and Joseph 1989). The percolation prototype distribution contains a single exponent up to a cutoff scale, more similar to the data interpretation in (Neggers et al. 2003). For very large clusters, the distribution cannot follow a power law with any exponent. This is due to the impossibility of producing infinite moments from a distribution of finite objects, as discussed after Eq. (3). In our case the size distribution changes dramatically as a function of the water vapor, with the expected rapid cutoff for low water vapor values and a substantial scale-free range for near-critical values. Most large clusters occur at near-critical values. Supercritical w values also generate large clusters, with the distribution dropping less steeply. However, these high w values occur infrequently (see Fig. 3), so the overall contribution remains relatively small. The weights of different water vapors in the overall distribution of cluster sizes can be read off Fig. 7 or 8 by comparing ranks or densities at the same area (looking up from a point on the abscissa).

For reference, the straight line corresponding to the exponent for two-dimensional critical percolation (in a homogeneous system) is included on the plot. While

underlining that no fit should be claimed here, we emphasize that cluster size distributions comparable in this respect to the statistics of MCSs can be produced by a model where clustering occurs not because of dynamics but simply because a number of pixels is forced into a two-dimensional space. For the reasons discussed above we are precluded from ascribing effects fully to percolation or to the physical transition. Nonetheless, the fact that cluster size distributions are “fat-tailed” should come as no surprise when clusters from the critical region are included in the statistics.

It has been argued that in an ensemble that includes both measurements in the critical region and measurements outside that region, it is possible to obtain cluster size distributions with exponents $\tau' > \tau$ larger than the “correct” critical value [cf. Eq. (3)], depending on the weight of measurements from the critical regime in the ensemble (Sornette 1994). This effect and the complicated spatial structure of the water vapor field modify the apparent exponent seen here and contribute to the observed dependence on water vapor. Percolation thus does not give a strong quantitative prediction for the behavior of the size distribution. Despite these complications, naively comparing the cluster size distribution to homogeneous percolation reveals a suggestive similarity, and stratifying the behavior by water vapor as is done here clearly helps in distinguishing different regimes of behavior. Attempting to infer functional forms of distributions by fitting data that combine different values of water vapor would lead to different conclusions, depending on whether a predominantly dry or moist area is being investigated. An exponential fits the distributions for low water vapor quite well, whereas broader distributions are needed for larger w values, with a power law yielding the best fit near criticality. Intriguingly, under different driving conditions in large-eddy simulations of shallow cumulus, some degree of universality was reported by Neggers et al. (2003), who constructed a dimensionless measure of cloud size by dividing by the characteristic cutoff scales of distributions.

6. Accessible hull scaling

Finally we examine the length of the accessible hull h , for which we have a robust prediction from the gradient percolation prototype discussed in the introduction. Specifically, we expect the accessible hull to be a fractal with dimension $d_f = 4/3$. The accessible hull consists of the pixels belonging to a cluster that are adjacent to empty pixels and can be reached from outside the cluster without having to pass through any narrow gates. It is thus a special kind of perimeter. We define a narrow gate

as an opening no wider than one pixel. On a grid that fully resolves the processes producing a cluster, a perimeter constructed without imposing the no-narrow-gates criterion would correspond to the full hull, whose dimension is $7/4$. For observations made at low resolution (relative to the small-scale physical processes generating the cluster), narrow gates are closed off automatically, preventing the full hull from being observed. In our case, at a coarse resolution of 5 km, we have confirmed that repeating our measurements without imposing the no-narrow-gates criterion yields very similar results (data not shown). However, given the difference in scaling, it seems important to impose the criterion to avoid any ambiguity, remarking that we expect the distinction between full hull and accessible hull to be important at higher spatial resolution.

We note that it is counterintuitive for a scaling property like the hull dimension to depend on the microscopic details of the hull definition. This subtle aspect has been treated in the mathematical physics literature and is now well understood. The difference between the full hull and the accessible hull was first pointed out by Grossman and Aharony (1986). For an in-depth discussion and illustrations, see also (Kolb 1990).

An easy way to test the predicted scaling is a comparison between cluster size and accessible hull length. The cluster is dense in its interior, with few holes. The area enclosed by the accessible hull is therefore approximately the cluster size. If the accessible hull is a fractal with dimension $4/3$, its length h will scale with cluster size s as $h \propto (s^{1/2})^{4/3}$. Figure 9 shows the median h as a function of $s^{1/2}$. The agreement with the asymptotic (large cluster) prediction from gradient percolation is very good for clusters consisting of more than about 10 pixels. Large clusters tend to be associated with high water vapor values and a gradient of $w(\mathbf{x})$ from interior to exterior, which is another reason why gradient percolation would apply particularly well here.

Under the argument above that coarse-resolution measurements of the perimeter tend to be effectively equivalent to the accessible hull, we can compare them to earlier area–perimeter scaling results for clouds or clusters (with the caveat that deviation toward the full hull scaling of $7/4$ might occur at high resolution). Results approximately consistent with the $4/3$ scaling have been repeatedly noted over various scale ranges (Lovejoy 1982; Cahalan and Joseph 1989; Benner and Curry 1998; Mapes and Houze 1993). Cahalan and Joseph (1989) wrote that “the slope [area–perimeter scaling] for those clouds between 100 m and 2 km is close to $4/3$,” while they found larger values for different cloud-detection thresholds and cloud types. These may reflect the crossover to $7/4$ scaling because they used data with

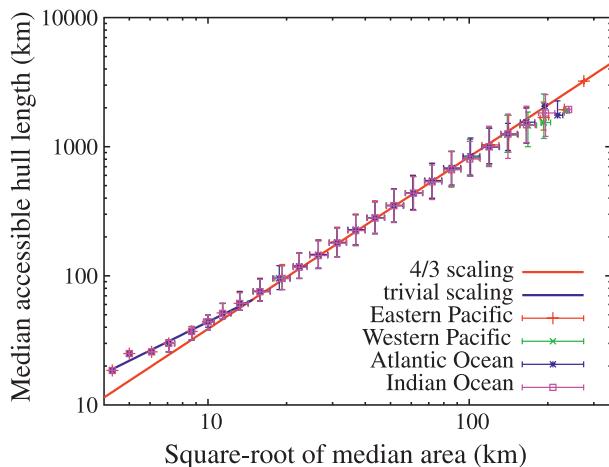


FIG. 9. Double-logarithmic plot of h (the length of the accessible hull) vs a linear scale, here the square root of the cluster size, \sqrt{s} . Data points are median values both for h and \sqrt{s} for each of the four regions. Vertical and horizontal bars span the 5th to 95th percentile range in each bin. These are not error bars; large clusters are so rare that the percentiles coincide, despite the uncertainty being large here. The red straight line has slope $4/3$, corresponding to the prediction from gradient percolation; the blue line represents trivial scaling, corresponding to a perimeter of dimension 1.

significantly higher spatial resolution and constructed a perimeter corresponding to the full hull.

Lovejoy (1982) used rain and cloud areas from satellite images and explicitly noted the proximity of the measured dimension to $4/3$: “The value 1.35 is so close to the value $4/3$ [...] An understanding of the physical origins of this value could therefore be important.” Mapes and Houze (1993) give 1.4 for IR-based cloud clusters, the Cahalan and Joseph (1989) ITCZ case yields values around 1.4–1.5, and Benner and Curry (1998) note 1.37 ± 0.06 for their larger clouds. The latter two references note a scale break to smaller values at $O(1 \text{ km})$, but they may be interpreted as indicating that the scaling that applies for MCSs may continue down to the scales of individual cloud plumes. Universality (as in the case of the fractal dimension) typically occurs in an intermediate-asymptotic regime (Barenblatt 1996)—that is, on scales that are large compared to their individual components, such as convective cells, and small compared to other constraints, such as large-scale variations in meteorological conditions. We summarize that a fractal dimension consistent with $4/3$ (with the caveat of some scatter in the estimates from various studies) in a scaling regime spanning about three orders of magnitude in linear cloud/cloud cluster size can be considered a well-established observation. Recognizing this, Siebesma and Jonker (2000) confirmed that the fractal dimension is reproduced in three-dimensional large-

eddy simulations of cumulus clouds. Their numerical procedure allowed them to compute volume–surface relations from the cloud bodies. Physical arguments were made to motivate these relations. Assuming isotropy, a two-dimensional projection of the three-dimensional objects would have a fractal dimension of $4/3$, and it was argued that reproducing such a nontrivial scaling relation is a strong test for model validity.

Geometric measures being dominated by percolation universality rather than physical processes is widely observed in two-dimensional lattice models (Fortunato 2002; Kertész 1989) and even two-dimensional turbulence (Bernard et al. 2006). This suggests an answer to the questions concerning the physical origins of the scaling and the discriminative power of the scaling in model testing. As in the systems cited above, the scaling for precipitation clusters appears to be dominated by geometric constraints rather than physical processes. A number of very different physical processes would produce the same value. Although this may be disappointing in terms of discriminative power in model testing, it suggests that simple representations of clusters are feasible in model parameterizations.

7. Discussion

As a key starting point, we confirmed qualitatively and quantitatively in TRMM radar data properties of tropical precipitation rate versus column water vapor w that were reported for microwave-inferred rain rates in PN06. These properties are consistent with those of a continuous phase transition. The power-law pickups of conditionally averaged precipitation rates as a function of water vapor exhibit critical water vapor values w_c for various tropical regions. The microwave-inferred critical values w_c^i and the power-law exponent β are compatible with the radar data.

As conjectured, the statistics of the precipitation clusters change strongly as a function of water vapor measured inside the cluster. The average size of the clusters and the average radius of gyration increase sharply near the transition point. The size distribution of precipitation clusters alters dramatically as a function of the water vapor. For low values of w the distribution decays fast for large clusters, whereas at very high water vapor, above the transition, the frequency of large clusters drops less quickly. The strong dependence on water vapor implies that studies of size distribution that do not account for this variable end up examining the weighted average of very different dependences. The frequency of occurrence of w (Fig. 3) does not have a universal form and can vary considerably among regions, which may provide an explanation for the different

functional forms of size distributions that have been suggested in the literature. By first stratifying by w , we examined whether there is a scale-free range at w values where theory would lead one to expect it (i.e., near the critical point of the precipitation transition) and this indeed appears to be the case. The exponent of the associated power law is sufficiently similar to that of the simplest protocol that yields such size distributions (i.e., two-dimensional percolation) that one might consider this a useful reference against which to test other hypotheses for the statistics of MCSs.

We note a number of ways in which the precipitation clusters differ from simple percolation. From the outset, we know that percolation cannot produce conventionally defined correlations such as those examined in PN06. Even when spanning clusters (spanning the radar swath) are removed from the sample, the average size does not decrease above the critical point, likely associated with inhomogeneity in the water vapor field. Clusters are fairly compact in the interior, as expected from meteorological observations (Houze 2004). The relationship between cluster size and the radius of gyration supports this; that is, large holes are rare. For values of w near and above criticality, which account for most of the large clusters, the cluster generally exists in a dryer environment, with a negative w gradient from the center outward. This suggests gradient percolation as a prototype model for the behavior of the cluster boundary. The robust scaling prediction from gradient percolation, an accessible hull dimension of $4/3$, was found to hold, in approximate agreement with perimeter estimates in previous studies (Lovejoy 1982; Cahalan and Joseph 1989; Mapes and Houze 1993; Benner and Curry 1998). An implication is that area–perimeter relations for cloud clusters may be largely independent of the physical processes involved. This weakens the case for model validation via comparison of area–perimeter relations (Siebesma and Jonker 2000).

Overall, these results support the usefulness of considering geometric aspects of mesoscale phenomena in terms of very simple models, provided the change in properties across the transition to strong convection is taken into account, here seen as a function of water vapor. Several statistical properties of the clusters are common to clusters in many other physical systems. This is a reflection of universality in critical phenomena and emphasizes the broad applicability of associated results.

Such coarse-grained knowledge can complement studies that focus on the particular physics of convective processes by providing prototypes or null hypotheses for certain features of the complex behavior, such as those mimicked by percolation with a probability dependent on the precipitable water. Of course, this must

be placed in context with studies of mesoscale physics: for instance, the clusters are seen here to depend strongly on precipitable water, but the water vapor field in turn depends strongly on the convection (e.g., Gamache and Houze 1983). Finally, we note that the scale-free range in the cluster size distribution near critical water vapor values extends across most of the range that can be examined with the TRMM radar resolution and swath width. Two traditional definitions of the mesoscale (Houze 1993; Mohr and Zipser 1996) here would imply cluster sizes greater than 500 km^2 and 2000 km^2 , but this size falls well within the scale-free range—features as small as a few $5 \text{ km} \times 5 \text{ km}$ boxes appear to be part of the same scaling behavior. This suggests that mesoscale clustering behavior is important over an even larger range of scales than traditionally considered.

Acknowledgments. This work was supported in part by the National Science Foundation Grant ATM-0645200, National Oceanic and Atmospheric Administration Grants NA05OAR431-1134, NA08OAR431-0882 (JDN and OP), and NA07OAR431-0214 (SN), and the Guggenheim Foundation (JDN). DN thanks J. L. Lin for asking what the PN06 results imply for cluster size distributions. OP would like to thank G. Pruessner, M. Gastner, and B. Oborny for helpful discussions on a related problem in ecology. We thank B. Stevens for discussions and R. Houze for comments on the manuscript.

REFERENCES

- Barenblatt, G. I., 1996: *Scaling, Self-Similarity, and Intermediate Asymptotics*. Cambridge University Press, 386 pp.
- Benner, T. C., and J. A. Curry, 1998: Characteristics of small tropical cumulus clouds and their impact on the environment. *J. Geophys. Res.*, **103** (D22), 28 753–28 767.
- Bernard, D., G. Bofetta, A. Celani, and G. Falkovich, 2006: Conformal invariance in two-dimensional turbulence. *Nature Phys.*, **2**, 124–128.
- Bretherton, C. S., M. E. Peters, and L. E. Back, 2004: Relationships between water vapor path and precipitation over the tropical oceans. *J. Climate*, **17**, 1517–1528.
- Cahalan, R. F., and J. H. Joseph, 1989: Fractal statistics of cloud fields. *Mon. Wea. Rev.*, **117**, 261–272.
- Cardy, J., 2005: SLE for theoretical physicists. *Ann. Phys.*, **318**, 81–118.
- Cheng, C.-P., and R. A. Houze Jr., 1979: The distribution of convective and mesoscale precipitation in GATE radar echo patterns. *Mon. Wea. Rev.*, **107**, 1370–1381.
- Coniglio, A., and W. Klein, 1980: Clusters and Ising critical droplets: A renormalization approach. *J. Phys.*, **13A**, 2775–2780.
- Cotton, W. R., and R. A. Anthes, 1989: *Storm and Cloud Dynamics*. Academic Press, 883 pp.
- Fortunato, S., 2002: Site percolation and phase transitions in two dimensions. *Phys. Rev. B*, **66**, 054107, doi:10.1103/PhysRevB.66.054107.

- Gamache, J. F., and R. A. Houze Jr., 1983: Water budget of a mesoscale convective system in the tropics. *J. Atmos. Sci.*, **40**, 1835–1850.
- Geerts, B., 1998: Mesoscale convective systems in the southeast United States during 1994–95: A survey. *Wea. Forecasting*, **13**, 860–869.
- Gouyet, J.-F., and M. Rosso, 2005: Diffusion fronts and gradient percolation: A survey. *Physica A*, **357**, 86–96.
- Grossman, T., and A. Aharony, 1986: Structure and perimeters of percolation clusters. *J. Phys.*, **19A**, L745–L751, doi:10.1088/0305-4470/19/12/009.
- Hilburn, K. A., and F. J. Wentz, 2008: Intercalibrated passive microwave rain products from the Unified Microwave Ocean Retrieval Algorithm (UMORA). *J. Appl. Meteor. Climatol.*, **47**, 778–794.
- Hinrichsen, H., 2000: Non-equilibrium critical phenomena and phase transitions into absorbing states. *Adv. Phys.*, **49**, 815–958.
- Houze, R. A., Jr., 1993: *Cloud Dynamics*. Academic Press, 573 pp.
- , 2004: Mesoscale convective systems. *Rev. Geophys.*, **42**, RG4003, doi:10.1029/2004RG000150.
- , and C.-P. Cheng, 1977: Radar characteristics of tropical convection observed during GATE: Mean properties and trends over the summer season. *Mon. Wea. Rev.*, **105**, 964–980.
- , D. C. Wilton, and B. F. Smull, 2007: Monsoon convection in the Himalayan region as seen by the TRMM Precipitation Radar. *Quart. J. Roy. Meteor. Soc.*, **133**, 1389–1411.
- Iguchi, T., T. Kozu, R. Meneghini, J. Awaka, and K. Okamoto, 2000: Rain-profiling algorithm for the TRMM precipitation radar. *J. Appl. Meteor.*, **39**, 2038–2052.
- Kertész, J., 1989: Existence of weak singularities when going around the liquid–gas critical point. *Physica A*, **161**, 58–62.
- Kolb, M., 1990: Crossover from standard to reduced hull for random percolation. *Phys. Rev.*, **41A**, 5725–5727.
- LeMone, M. A., E. J. Zipser, and S. B. Trier, 1998: The role of environmental shear and thermodynamic conditions in determining the structure and evolution of mesoscale convective systems during TOGA COARE. *J. Atmos. Sci.*, **55**, 3493–3518.
- López, R. A., 1977: The lognormal distribution and cumulus cloud populations. *Mon. Wea. Rev.*, **105**, 865–880.
- Lovejoy, S., 1982: Area–perimeter relation for rain and cloud areas. *Science*, **216**, 185–187.
- Lucas, C., E. J. Zipser, and B. S. Ferrier, 2000: Sensitivity of tropical west Pacific oceanic squall lines to tropospheric wind and moisture profiles. *J. Atmos. Sci.*, **57**, 2351–2373.
- Mapes, B. E., and R. A. Houze Jr., 1993: Cloud clusters and superclusters over the oceanic warm pool. *Mon. Wea. Rev.*, **121**, 1398–1415.
- Mohr, K. I., and E. J. Zipser, 1996: Mesoscale convective systems defined by their 85-GHz ice scattering signature: Size and intensity comparison over tropical oceans and continents. *Mon. Wea. Rev.*, **124**, 2417–2437.
- Moloney, N. R., and G. Pruessner, 2003: Asynchronously parallelized percolation on distributed machines. *Phys. Rev.*, **67E**, 037701, doi:10.1103/PhysRevE.67.037701.
- Neggers, R. A. J., H. J. J. Jonker, and A. P. Siebesma, 2003: Size statistics of cumulus cloud populations in large-eddy simulations. *J. Atmos. Sci.*, **60**, 1060–1074.
- Nesbitt, S., R. Cifelli, and S. A. Rutledge, 2006: Storm morphology and rainfall characteristics of TRMM precipitation features. *Mon. Wea. Rev.*, **134**, 2702–2721.
- Peters, O., and J. D. Neelin, 2006: Critical phenomena in atmospheric precipitation. *Nature Phys.*, **2**, 393–396.
- Siebesma, A. P., and H. J. J. Jonker, 2000: Anomalous scaling of cumulus cloud boundaries. *Phys. Rev. Lett.*, **85**, 214–217.
- Sornette, D., 1994: Sweeping of an instability: An alternative to self-organized criticality to get power laws without parameter tuning. *J. Phys. I France*, **4**, 209–221.
- Stauffer, D., and A. Aharony, 1994: *Introduction to Percolation Theory*. 2nd ed. Taylor and Francis, 181 pp.
- Tompkins, A. M., 2001: Organization of tropical convection in low vertical wind shears: The role of water vapor. *J. Atmos. Sci.*, **58**, 529–545.
- Wentz, F. J., and R. W. Spencer, 1998: SSM/I rain retrievals within a unified all-weather ocean algorithm. *J. Atmos. Sci.*, **55**, 1613–1627.
- Williams, M., and R. A. Houze Jr., 1987: Satellite-observed characteristics of winter monsoon cloud clusters. *Mon. Wea. Rev.*, **115**, 505–519.